Inorg. Chem. **2002**, *41*, 2826–2833

Detection and Measurement of Noncoincidence between the Principal Axes of the g-Matrix and Zero-Field Splitting Tensor Using Multifrequency Powder EPR Spectroscopy: Application to *cis*-$[(NH_3)_2Pt(1\text{-}MeU)_2Cu(H_2O)_2](SO_4)\cdot 4.5H_2O$ (1-MeU = Monoanion of 1-Methyluracil)

David Collison,[†] David M. L. Goodgame,[‡] Michael A. Hitchman,[§] Bernhard Lippert,[||] Frank E. Mabbs,[†] and Eric J. L. McInnes*,[†]

EPSRC c.w. EPR Service Centre, Chemistry Department, The University of Manchester, Manchester, M13 9PL, U.K., Chemistry Department, Imperial College of Science, Technology and Medicine, London, SW7 2AY, U.K., School of Chemistry, University of Tasmania, GPO Box 252-75, Hobart Tasmania 7001, Australia, and Lehrstuhl für Anorganische Chemie III, Fachbereich Chemie, Universität Dortmund, 44221 Dortmund, Germany

Received December 14, 2001

Multifrequency continuous wave EPR spectra (4–34 GHz) on a powder of the title compound are consistent with a spin-triplet state. This arises from interaction between centrosymmetrically related pairs of copper(II) ions in the solid. The spectra at all frequencies have been simulated with a single set of spin-Hamiltonian parameters. The results show that there is noncoincidence between the principal axes of the **g**-matrices on each copper center and those of the zero-field splitting (**D**) tensor. This noncoincidence is a single rotation of 33° ± 2°. The parameters from the powder spectra have been verified by a subsequent single-crystal EPR study which yielded the spin-Hamiltonian parameters $g_{XX} = 2.074$, $g_{YY} = 2.093$, $g_{ZZ} = 2.385$, $D_{XX} = \pm 0.0228$ cm^{-1}, $D_{YY} = \pm 0.0211$ cm^{-1}, $D_{ZZ} = \mp 0.0439$ cm^{-1} with Euler angles of $\alpha = 179°$, $\chi = 33.4°$, and $\gamma = 328°$. Analysis of the zero-field splitting tensor in terms of exchange indicates that the interaction between the pairs of copper(II) ions is almost entirely dipolar in origin. This study shows that multifrequency EPR spectroscopy on powders, coupled with spectrum simulation, can detect *and* measure noncoincidence between the principal axes of the **g**-matrix and zero-field splitting tensor, and does not necessarily require the presence of metal hyperfine interactions.

Introduction

We have an interest in the noncoincidence between the principal axes of the **g**-matrix and metal hyperfine matrix in monomeric d-transition metal complexes.[1−9] Where such noncoincidence occurs, it arises from low site symmetry at the metal. For spin doublets it has been possible in some examples to measure the angles of noncoincidence from powder EPR measurements using multifrequency spectra, along with computer simulations.[2,3,8] Although the best way to determine the angles of noncoincidence is by single-crystal EPR, we have found good agreement between the results from powder and single-crystal spectra, where both types

* Author for correspondence. E-mail: eric.mcinnes@man.ac.uk.
† The University of Manchester.
‡ Imperial College of Science, Technology and Medicine.
§ University of Tasmania.
|| Universität Dortmund.

(1) Gahan, B.; Howlader, N. C.; Mabbs, F. E. *J. Chem. Soc., Dalton Trans.* **1981**, 142.
(2) Collison, D.; Mabbs, F. E.; Enemark, J. H.; Cleland, W. E., Jr. *Polyhedron* **1986**, *5*, 423.
(3) Young, C. G.; Enemark, J. H.; Collison, D.; Mabbs, F. E. *Inorg. Chem.* **1987**, *26*, 2925.
(4) Collison, D.; Gahan, B.; Mabbs, F. E. *J. Chem. Soc., Dalton Trans.* **1987**, 111.
(5) Collison, D.; Mabbs, F. E.; Temperley, J.; Christou G.; Huffman, J. C. *J. Chem. Soc., Dalton Trans.* **1988**, 309.
(6) Collison, D.; Mabbs, F. E.; Temperley, J. *Spectrochimica Acta* **1991**, *47A*, 691.
(7) Collison, D.; Mabbs, F. E.; Rigby, K.; Cleland, W. E., Jr. *J. Chem. Soc., Faraday Trans.* **1993**, *89*, 3695.
(8) Collison, D.; Eardley, D. R.; Mabbs, F. E.; Rigby, K.; Bruck, M. A.; Enemark, J. H.; Wexler, P. A. *J. Chem. Soc., Dalton Trans.* **1994**, 1003.
(9) McInnes, E. J. L.; Mabbs, F. E.; Harben, S. M.; Smith, P. D.; Collison, D.; Garner, C. D. Smith, G. M.; Riedi, P. C. *J. Chem. Soc., Faraday Trans.* **1998**, *94*, 3013.

10.1021/ic011283e CCC: $22.00
Published on Web 05/07/2002

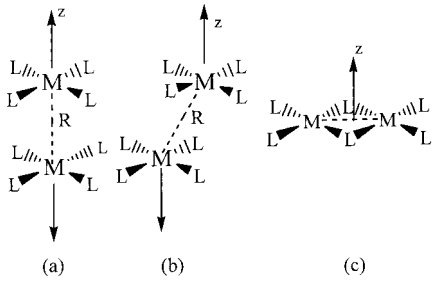

Figure 1. Three common arrangements found in dimers formed from square planar ML_4 monomers (R = M···M separation).

of measurement have been possible on the *same* materials.[4,5,7−9] This gives confidence in the findings from powder data alone.

In the case of spin states with $S > {}^1/_2$, zero-field splitting (ZFS, **D**) effects are usually present. Spin states with $S > {}^1/_2$ result from multiple unpaired electrons in monomeric systems or from spin states generated from exchange interactions in polymeric systems. As with **g**-matrices and hyperfine matrices in spin doublets, noncoincidence between the **g**-matrix and the **D**-tensor is possible when $S > {}^1/_2$. In monomeric systems the noncoincidence will be a consequence of low site symmetry. For such spin states in polymeric systems, the noncoincidence may occur when the principal axes of the **g**-matrices on the individual centers are not coparallel and/or when the principal directions of the anisotropic exchange or dipolar interaction are not the same as those of the **g**-matrices.[10]

Bencini and Gatteschi[10] have indicated three common arrangements for copper(II) binuclear compounds, see Figure 1. In this figure, arrangement a has the **g**-matrices on the two centers coparallel. This situation is exemplified[11] by $[Cu(acetate)_2(H_2O)]_2$. In this case the principal axes of the **g**-matrix and the **D**-tensor coincide. The situation illustrated in Figure 1c could result in noncoincidence between the largest components of **g** and **D**, particularly when the dipolar and anisotropic exchange contributions to **D** are similar in magnitude. An example of this is shown from the single-crystal EPR of the pyridine *N*-oxide (pyNO) complexes, $[Cu(pyNO)Cl_2(H_2O)]_2$ and $[Cu(pyNO)Cl_2(pyNO)]_2$, where angles of noncoincidence of 24° and 27°, respectively, were found.[12,13] However, the powder EPR spectra were not reported. The example in Figure 1b is relevant to *cis*-$[(NH_3)_2Pt(1\text{-}MeU)_2Cu(H_2O)_2](SO_4)\cdot 4.5H_2O$,[14,15] the compound studied in this paper. This compound exists as a centrosymmetrically related pair of cations in the solid state, see Figure 2a. The $\{CuO_2Cu\}$ core of this dimeric arrangement is that of a rhombus with unsymmetrical bridging of the oxygen atoms from the monoanion of 1-methyluracil, as shown in

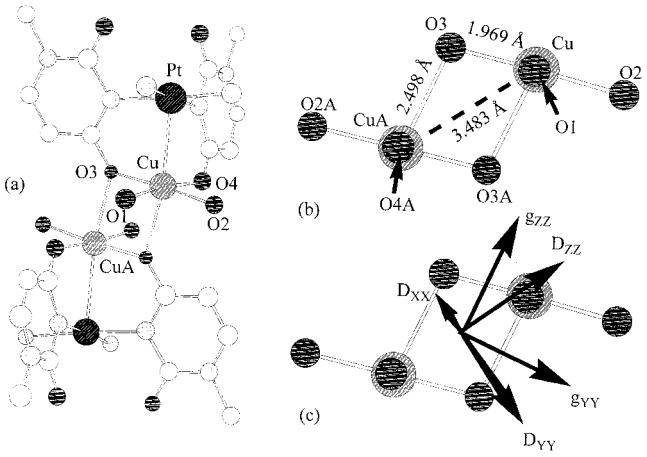

Figure 2. Representation of (a) the whole and (b) the dicopper entity in the centrosymmetric dimeric unit in the crystal of *cis*-$[(NH_3)_2Pt(1\text{-}MeU)_2Cu(H_2O)_2](SO_4)\cdot 4.5H_2O$. (c) View down g_{XX} showing the orientation of the principal *g*- and *D*-values from the single-crystal EPR study.

Figure 2b. There is no element of symmetry at the Cu center. As we will demonstrate later, via both multifrequency powder and single-crystal EPR, there is a spin triplet state in which there is noncoincidence between the **D**-tensor and the **g**-matrices on each copper(II) center.

Although there are a number of examples of the measurement of the noncoincidence between the **g**-matrix and **D**-tensors from single-crystal measurements, there is, to the best of our knowledge, very little information concerning the effects of this noncoincidence on powder EPR spectra. Pilbrow et al. published a series of papers[16−19] in which simulations of X-band EPR spectra of polycrystalline dimeric complexes were used to determine metal−metal distances and relative orientations of the metal centers. However, the methods used are essentially sequential perturbation treatments involving the metal hyperfine interaction and the ZFS. Furthermore, it was assumed that the ZFS was entirely dipolar in origin. There is also a report by Golding and Tennant[20] who used a sequential perturbation approach to derive analytical expressions for the resonance fields. This approach is valid when the ZFS is smaller in energy than the electronic Zeeman effect. However, the only information presented consisted of the effect of varying a single angle of noncoincidence for a fixed set of **g**-matrices and **D**-tensors and a single microwave frequency. Although these results illustrate some interesting features arising from noncoincidence, they do not address the problem that, *given a set of powder EPR spectra, how can we tell if there is noncoincidence or not?* Pilbrow et al. used the successful simulation of the spectra, including the observed hyperfine structure, to determine the distance between, and the relative orientation of, the metal−metal vectors. The results were then compared

(10) Bencini, A.; Gatteschi, D. *EPR of Exchange Coupled Systems*; Springer-Verlag: Berlin, 1990; Chapters 2 and 3.
(11) (a) Bleaney, B.; Bowers, K. D. *Philos. Mag.* **1952**, *43*, 372. (b) Bleaney, B.; Bowers, K. D. *Proc. R. Soc. London* **1952**, *A214*, 451. (c) Abe, H.; Shimada, J. *Phys. Rev.* **1953**, *90*, 316. (d) Abe, H.; Shimada, J. *J. Phys. Soc. Jpn.* **1957**, *12*, 1255.
(12) Kokoska, G. F.; Allen, Jr., H. C.; Gordon, G. *J. Chem. Phys.* **1967**, *46*, 3013.
(13) Kokoska, G. F.; Allen, Jr., H. C.; Gordon, G. *J. Chem. Phys.* **1967**, *46*, 3020.
(14) Lippert, B.; Thewalt, U.; Schollhorn, H.; Goodgame, D. M. L.; Rollins, R. W. *Inorg. Chem.* **1984**, *23*, 2807.
(15) Neugebauer, D.; Lippert, B. *J. Am. Chem. Soc.* **1982**, *104*, 6596.
(16) Boas, J. F.; Pilbrow, J. R.; Hartzell, C. R.; Smith, T. D. *J. Chem. Soc. A* **1969**, 572.
(17) Boas, J. F.; Pilbrow, J. R.; Smith, T. D. *J. Chem. Soc. A* **1969**, 723.
(18) Boyd, P. D. W.; Smith, T. D.; Price, J. H.; Pilbrow, J. R. *J. Chem. Phys.* **1972**, *56*, 1253.
(19) Boyd, P. D. W.; Toy, A. D.; Smith, T. D.; Pilbrow, J. R. *J. Chem. Soc., Dalton Trans.* **1973**, 1549.
(20) Golding, R. M.; Tennant, W. C. *Mol. Phys.* **1973**, *25*, 1163.

with appropriate solid state structures to confirm the interpretation. However, spectra were only obtained at X-band frequency. Our experience with spin-triplets is that it is usually possible to obtain an acceptable simulation of a powder spectrum at a *single frequency* with a given set of spin-Hamiltonian parameters with coincident principal axes of the **g**-matrix and **D**-tensor, especially when the EPR lines are broad. However, using this same set of parameters at a different frequency can result in a poor simulation of the experimental spectrum. This need to use different spin-Hamiltonian parameters to fit powder spectra at different frequencies can be a sign of the presence of noncoincidence between the **D**-tensor and **g**-matrix. The aim of this paper is to illustrate how this noncoincidence may be detected and measured using multifrequency powder EPR spectra coupled with spectrum simulation. Although we use a binuclear copper(II) species as our example, the main conclusions are also applicable to other spin triplets.

Experimental Section

cis-$[(NH_3)_2Pt(1\text{-}MeU)_2Cu(H_2O)_2](SO_4)\cdot 4.5H_2O$ was prepared and crystallized as reported previously (unit cell parameters: space group $P\bar{1}$, $a = 10.398$ Å, $b = 10.773$ Å, $c = 11.772$ Å, $\alpha = 102.88°$, $\beta = 102.62°$, $\gamma = 105.05°$).[14,15]

EPR Spectroscopy. EPR spectra of the powdered solid of *cis*-$[(NH_3)_2Pt(1\text{-}MeU)_2Cu(H_2O)_2](SO_4)\cdot 4.5H_2O$ were recorded at room temperature at ca. 4 (S), 9.5 (X), 24 (K), and 34 GHz (Q-band) and down to 5 K at 24 GHz using a Bruker ESP 300E spectrometer. The magnetic fields were calibrated with a Bruker ER035M Gaussmeter and the microwave frequencies measured with an EIP588C microwave counter. Modulation frequencies and amplitudes of 100 kHz and 10 G, respectively, were used. The spectra measured at room temperature are shown in Figure 3. Single-crystal X-band EPR spectra at room temperature were obtained in three mutually orthogonal planes, with reference to the axes in Figure 4 on a crystal (ca.1 × 0.5 × 0.2 mm) mounted on quartz studs. The data were analyzed using the methods of Schönland,[21] and of Lund and Vänngård[22] to give the directions of the **g**-matrix and **D**-tensor with respect to the measuring axes (see later for justification of this method). The results are summarized in Table 1.

EPR Simulations. There are two approaches to the simulation of the powder spectra of a dimer. One is to make no assumption concerning the relative magnitudes of the electronic Zeeman interaction, the metal hyperfine interaction, the isotropic exchange, or the ZFS. The spin-Hamiltonian which expresses these interactions between the metal ions is[23,24]

$$\mathrm{H} = J\hat{\mathrm{S}}(1)\cdot\hat{\mathrm{S}}(2) + \beta_e\underline{\mathrm{B}}\cdot\mathbf{g}(1)\cdot\hat{\mathrm{S}}(1) + \beta_e\underline{\mathrm{B}}\cdot\mathbf{g}(2)\cdot\hat{\mathrm{S}}(2) + \hat{\mathrm{S}}(1)\cdot\mathbf{A}'(1)\cdot\hat{\mathrm{I}}(1) + \hat{\mathrm{S}}(2)\cdot\mathbf{A}'(2)\cdot\hat{\mathrm{I}}(2) + \hat{\mathrm{S}}(1)\cdot\mathbf{J}'\cdot\hat{\mathrm{S}}(2) \quad (1)$$

where B is the applied magnetic field, $\mathbf{g}(1)$, $\mathbf{g}(2)$, $\mathbf{A}'(1)$, and $\mathbf{A}'(2)$ are the **g**- and **A′**-matrices on centers 1 and 2, respectively, J is the isotropic exchange parameter, and $\mathbf{J}'$ is the anisotropic exchange tensor. The anisotropic exchange is responsible for the ZFS in this formalism.

Alternatively, one can assume that the isotropic exchange coupling is significantly larger than the microwave energy being used so that a spin-singlet and a spin-triplet result. The energy separation between these two states is much larger than the microwave energy, and the EPR spectrum arises from transitions within the spin-triplet only. This situation can be represented by the spin-Hamiltonian,

$$\mathrm{H} = \beta_e\underline{\mathrm{B}}\cdot\mathbf{g}\cdot\hat{\mathrm{S}} + \hat{\mathrm{S}}\cdot\mathbf{D}\cdot\hat{\mathrm{S}} + \hat{\mathrm{S}}\cdot\mathbf{A}\cdot\hat{\mathrm{I}} \quad (2)$$

or its more commonly used form,

$$\mathrm{H} = \beta_e\underline{\mathrm{B}}\cdot\mathbf{g}\cdot\hat{\mathrm{S}} + D[\hat{\mathrm{S}}_z^2 - S(S+1)/3] + E[\hat{\mathrm{S}}_x^2 + \hat{\mathrm{S}}_y^2] + \hat{\mathrm{S}}\cdot\mathbf{A}\cdot\hat{\mathrm{I}} \quad (3)$$

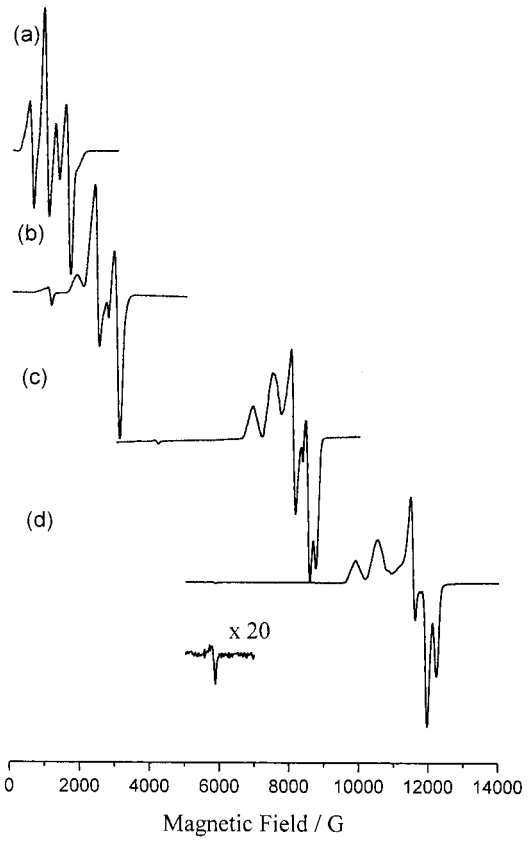

Figure 3. Room temperature, powder EPR spectra of *cis*-$[(NH_3)_2Pt(1\text{-}MeU)_2Cu(H_2O)_2](SO_4)\cdot 4.5H_2O$ at (a) S-band (3.862 GHz), (b) X-band (9.449 GHz), (c) K-band (24.216 GHz), and (d) Q-band (33.886 GHz).

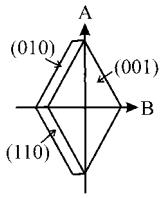

Figure 4. The crystal morphology and the measurement axes (*A*, *B*, and $C = B \times A$) used for the single-crystal EPR study.

Table 1. The Principal Values of the **g**-Matrix and **D**-Tensor (D_{ij} Elements in cm^{-1}) and their Relative Orientations (deg) from the Single-Crystal EPR Study[a]

	$D_{ZZ} = \mp 0.0439$	$D_{YY} = \pm 0.0211$	$D_{XX} = \pm 0.0228$
$g_{XX} = 2.074$	89.4	122.6	147.4
$g_{YY} = 2.093$	56.6	134.4	63.0
$g_{ZZ} = 2.385$	33.4	62.0	106.8

[a] These angles correspond to Euler angles of $a = 179°$, $\chi = 33.4°$, and $\gamma = 328°$.

(21) Schönland, D. S. *Proc. Phys. Soc., London* **1959**, *73*, 788.
(22) Lund, A.; Vänngård, T. *J. Chem. Phys.* **1965**, *42*, 2979.
(23) Abragam, A.; Bleaney, B. *Electron Paramagnetic Resonance of Transition Ions*; Clarendon Press: Oxford, 1970; Chapter 9.
(24) Mabbs, F. E.; Collison, D. *Mol. Phys. Rep.* **1999**, *26*, 39.

The correspondence[23] between D_{ii} in eq 2 and J'_{ii} in eq 1 is $J'_{ii} = 2D_{ii}$, with the result that, in Hamiltonian 3, $D = 3J'_{ZZ}/4$ and $E = (J'_{XX} - J'_{YY})/4$. Similarly, the relationship between the hyperfine interaction for the individual centers (**A′**) and for the dimer (**A**) is $A'_{ii} = 2A_{ii}$.

In order to make our simulation software general we based it on the spin-Hamiltonian in eq 1 using the techniques described previously.[25] The program makes no assumptions concerning the relative magnitudes of the various interactions in eq 1 and therefore uses matrix diagonalization techniques, based on this spin-Hamiltonian and the product spin functions $|S(1),S(2),M_S(1),M_S(2),I(1),I(2),M_I(1),M_I(2)\rangle$, to obtain the eigenvalues and eigenfunctions required to calculate the resonance positions and intensities. In order that the method has general applicability, the possibility of transitions occurring between all pairs of eigenstates is considered. Also the mutual orientations of the principal axes of the **g**- and **A′**-matrices and the **J′**-tensor can be noncoincident. However, for the simulations in this work we have assumed that $J \gg J'$ (i.e., we have "first-order" triplet spectra, see later), and for simplicity we discuss the ZFS and hyperfine interactions in terms of D and A rather than J' and A', where $D_{ii} = J'_{ii}/2$ and $A_{ii} = A'_{ii}/2$. The simulation program was run on a Digital 200/4/233 Alpha Workstation.

Results

When we set out to study *cis*-$[(NH_3)_2Pt(1\text{-}MeU)_2Cu(H_2O)_2](SO_4)\cdot 4.5H_2O$, we were initially unable to isolate a single crystal suitable for EPR studies and we were limited to analysis of powder EPR data alone. Eventually, we did isolate a crystal suitable for single crystal studies, and these results largely confirmed our powder analysis. In the following we detail these two sets of measurements separately, in order to emphasize that noncoincidence effects can be measured and determined from powder data *alone*.

Multifrequency Powder Spectra. The experimental EPR spectra of *cis*-$[(NH_3)_2Pt(1\text{-}MeU)_2Cu(H_2O)_2](SO_4)\cdot 4.5H_2O$ (Figure 3) are typical of those expected for a spin-triplet state wherein the ZFS is smaller than the applied microwave energies in all cases. Note that the "half-field" formally spin-forbidden transition becomes relatively more intense with decreasing microwave frequency as expected.[26] Attempts to simulate the spectra assuming *coincident* axes for the **g**-matrix and **D**-tensor soon showed that a *single set* of spin-Hamiltonian parameters did not give satisfactory simulations at *all* frequencies. An illustration of the discrepancies in the simulated versus experimental spectra is given in Figures 5−8, where spectra a and b are the simulated and experimental spectra, respectively. (The weak signals marked † in the experimental spectra are due to traces of isolated $S = {}^1/_2$ centers. Spectra c and d in Figures 5−8 are simulations based on models incorporating noncoincidence, see later.) Here, at each frequency, we have used the spin-Hamiltonian parameters that gave a reasonable simulation of the S-band spectrum (Figure 5a,b). The discrepancies between the simulated and experimental spectra become larger as the frequency increases. Similarly, a good simulation could be obtained for the Q-band spectrum using coincident axes, *but* the same parameters gave poor simulations at the lower frequencies. We have taken this to suggest that the assumption of coincident axes is incorrect. Thus, attempts were made to simulate the spectra with noncoincidence between the **g**-matrix and **D**-tensor.

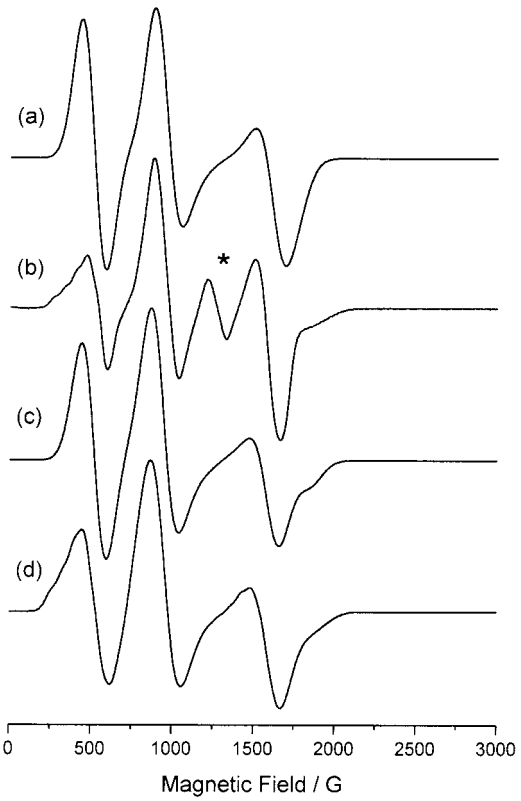

Figure 5. Room temperature S-band powder EPR spectra of *cis*-$[(NH_3)_2Pt(1\text{-}MeU)_2Cu(H_2O)_2](SO_4)\cdot 4.5H_2O$: (a) simulation with coincident axes and $g_{XX} = 2.06$, $g_{YY} = 2.08$, $g_{ZZ} = 2.37$, $D_{XX} = 0.022$ cm^{-1}, $D_{YY} = 0.022$ cm^{-1}, $D_{ZZ} = -0.044$ cm^{-1}; (b) experimental; (c) simulation with noncoincident axes, excluding copper hyperfine, and $g_{XX} = 2.06$, $g_{YY} = 2.08$, $g_{ZZ} = 2.37$, $D_{XX} = 0.022$ cm^{-1}, $D_{YY} = 0.022$ cm^{-1}, $D_{ZZ} = -0.044$ cm^{-1} with a 33° rotation about g_{XX}/D_{XX}; (d) simulation with noncoincident axes, including copper hyperfine with $A_{ZZ} = 0.0070$ cm^{-1}, $A_{XX} = A_{YY} = 0.0005$ cm^{-1} and the other parameters as in spectrum c. The feature marked * is not reproduced by the simulations.

Because the crystal structure consists of centrosymmetrically related molecules, it is required that the principal axes of the **g**-matrices on each copper ion are mutually parallel. We would expect the largest g-value (g_{ZZ}) to be approximately perpendicular to the CuO_4 coordination plane (see Figure 2c). Note, we use X, Y, Z for convenience to denote the principal axis system of each individual interaction, and hence this is *not* a common reference framework. In the assumption that the exchange between the two Cu(II) ions is largely dipolar we would expect the largest component of the **D**-tensor (D_{ZZ}) to be approximately along the Cu···Cu vector, and thus we might expect g_{ZZ} and D_{ZZ} to be nonparallel. Therefore, we attempted to model the powder EPR spectra with a single (i.e., monoclinic) twist about the axis perpendicular to the Cu_2O_2 plane. After several trial and error simulations it became apparent that a single rotation of the principal **D**-tensor about an axis parallel to the smallest g-value gives good simulations at *all* frequencies. The final

(25) Mabbs, F. E.; Collison, D. *Electron Paramagnetic Resonance of d Transition Metal Compounds*; Elsevier: Amsterdam, 1992; Chapters 7 and 16.
(26) Eaton, S. S.; More, K. M.; Sawant, B. M.; Eaton, G. R. *J. Am. Chem. Soc.* **1983**, *105*, 6560.

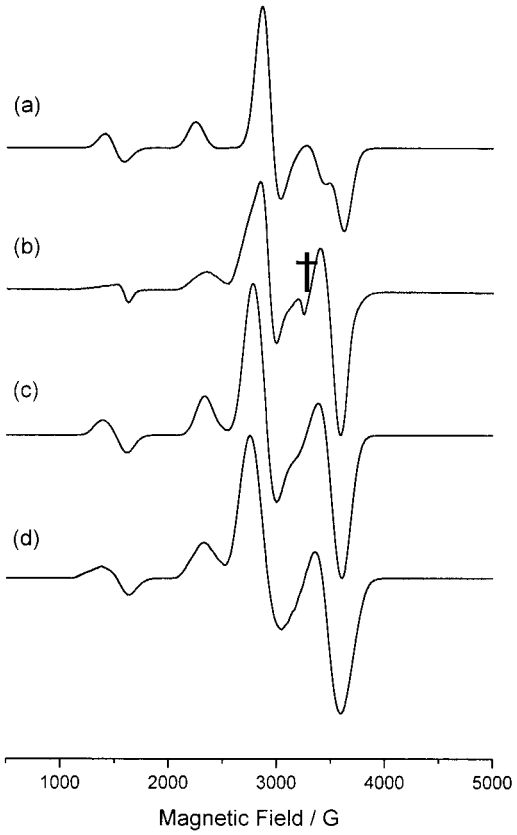

Figure 6. Room temperature X-band powder EPR spectra of *cis*-$[(NH_3)_2Pt(1\text{-}MeU)_2Cu(H_2O)_2](SO_4)\cdot 4.5H_2O$: (a−d) as in Figure 5. The feature marked † is due to isolated $S = {}^1/_2$ centers.

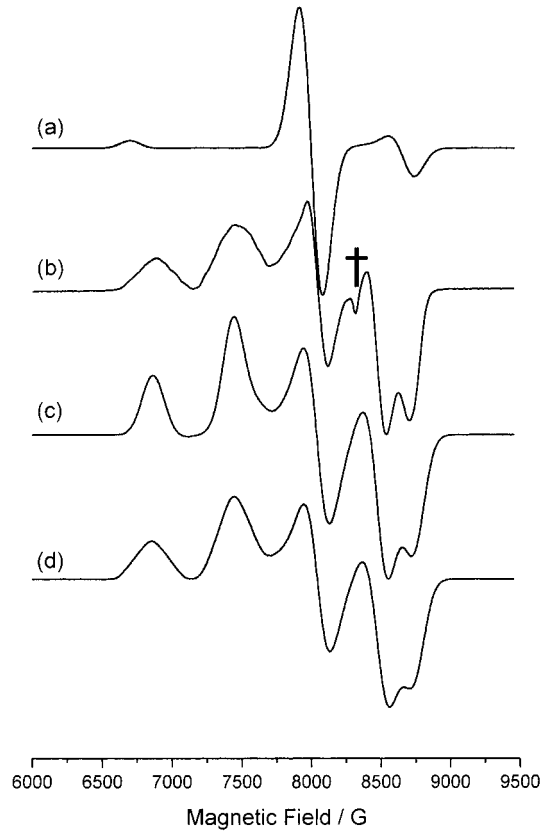

Figure 7. Room temperature K-band powder EPR spectra of *cis*-$[(NH_3)_2Pt(1\text{-}MeU)_2Cu(H_2O)_2](SO_4)\cdot 4.5H_2O$: a−d as in Figure 5. The feature marked † is due to isolated $S = {}^1/_2$ centers.

simulations, using a *consistent* set of spin-Hamiltonian parameters, are shown in Figures 5c to 8c. The principal values of g and D used were $g_{XX} = 2.06$, $g_{YY} = 2.08$, $g_{ZZ} = 2.37$, $D_{XX} = \pm 0.022$ cm^{-1}, $D_{YY} = \pm 0.022$ cm^{-1}, $D_{ZZ} = \mp 0.044$ cm^{-1} with a 33° ± 2° twist about g_{XX} (D_{XX}). The simulations, with respect to both the positions and relative intensities of the features compared with the experimental spectra, are good at *all* the frequencies studied. However, these simulations did not give very convincing line shapes. The inclusion of a hyperfine splitting of magnitude $A_{ZZ} = 0.0070$ cm^{-1} and $A_{XX} = A_{YY} = 0.0005$ cm^{-1} with coincident principal axes to the **g**-matrix gave the simulated spectra in Figures 5d to 8d [note that A_{XX} and A_{YY} are not resolved and we have assumed values typical for square planar Cu(II)].[27] The spectral profiles are much closer to those found in the experimental spectra. The **D**-tensor, transformed to be parallel to the g-frame on either copper center (coordinate frame x, y, z), is in Appendix 1a.

Single-Crystal Spectra. In all three orthogonal planes the spectra consisted of a pair of lines, the separation between which varied with the angle with respect to the applied magnetic field. This behavior is consistent with a spin-triplet state. The magnitudes of these separations correspond to the ZFS, which is considerably smaller than the X-band microwave energy of the experiment. Thus it is permissible to use the perturbation approach of Schönland[21] and of Lund and Vänngård[22] based on the spin-Hamiltonian in eq 2, to analyze the data. At a small number of orientations, close to where there was a maximum in the separation between the two lines, seven-line copper hyperfine multiplets were observed. The maximum hyperfine splitting was ca. 70 G, and we take this to be associated with g_{ZZ} for the dimer.

In the above analysis there is an ambiguity in the relative signs of off-diagonal elements in the crystal **g**-matrix and **D**-tensor, which initially gives two sets of spin-Hamiltonian parameters.[25] We were able to eliminate one of these sets, because the parameters gave simulated powder spectra which were incompatible with experiment. The alternative set [$g_{XX} = 2.074$, $g_{YY} = 2.093$, $g_{ZZ} = 2.385$, $D_{XX} = \pm 0.0228$ cm^{-1}, $D_{YY} = \pm 0.0211$ cm^{-1}, $D_{ZZ} = \mp 0.0439$ cm^{-1} with Euler angles[28] of $\alpha = 179°$, $\chi = 33.4°$, and $\gamma = 328°$] gives powder spectra simulations almost identical to those in Figures 5−8d. Within this preferred set, there are four possible choices of the orientations of the **g**-matrix and **D**-tensor with respect to the molecular geometry.[25] Two of these possibilities have the largest g-value (g_{ZZ}) lying approximately *within* the CuO_4 coordination plane, and we discard these solutions: we would expect g_{ZZ} to be approximately perpendicular to the CuO_4 plane.[27] The two remaining solutions have g_{ZZ} at an angle of 15.5° and 25.6° to the normal of the best plane through CuO_4 and at an angle of 12.1° and 19.6°, respectively, to the Cu−Pt vector. We favor the former solution because it gives g_{ZZ} significantly closer to the normal of the CuO_4 plane.

(27) Maki, A. H.; McGarvey, B. R. *J. Chem. Phys.* **1952**, *29*, 31.

(28) Mabbs, F. E.; Collison, D. *Electron Paramagnetic Resonance of d Transition Metal Compounds*; Elsevier: Amsterdam, 1992; p 1199.

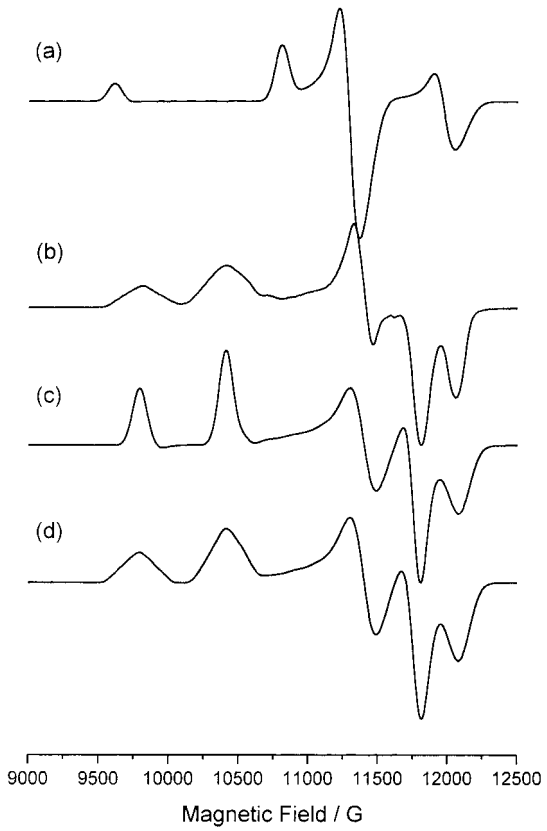

Figure 8. Room temperature Q-band powder EPR spectra of *cis*-$[(NH_3)_2Pt(1\text{-}MeU)_2Cu(H_2O)_2](SO_4)\cdot 4.5H_2O$: a−d as in Figure 5.

Table 2. Angles (deg) between the Principal Values of the **g**-Matrix and **D**-Tensor and Selected Molecular Directions

principal value	Cu−CuA	Cu−Pt	Cu−O1	Cu−O4	Cu−O2	Cu−O3	Cu−O3A
g_{XX}	85.8	74.6	172.2	14.0	99.9	82.7	89.9
g_{YY}	118.2	113.1	94.1	80.8	16.0	162.4	84.6
g_{ZZ}	135.2	19.6	83.6	102.3	91.5	90.8	168.1
D_{ZZ}	176.3	57.8	88.3	92.9	43.4	139.1	142.7
D_{YY}	87.3	60.6	55.2	131.4	127.9	51.9	114.8
D_{XX}	97.0	128.1	43.9	129.7	52.7	123.9	74.4

However, the deviation of g_{ZZ} from the normal is still surprisingly large, and we propose that this deviation is due to the presence of the Pt(II) ion in the axial position (2.765 Å). The Cu−Pt vector makes an angle of 12.1° to the normal to the CuO_4 plane.

With this solution, we find that g_{XX} (=2.074) is close to being parallel to the Cu−O4, Cu−O1 directions, while g_{YY} (=2.093) is close to parallel with the Cu−O2, Cu−O3 directions. Hence these *g*-values are equated with the local g_{xx}, g_{yy}, and g_{zz} on the individual copper centers. The *g*-values are similar to those used to simulate the powder spectra and to those reported[14] for the X- and Q-band powder EPR spectra of the related compound, *cis*-$[(NH_3)_2Pt(1\text{-}MeU)(1\text{-}MeC)Cu(1\text{-}MeC)(1\text{-}MeU)Pt(NH_3)_2]^{4+}$, in which the copper(II) ions are isolated from each other in the solid state. The final spin-Hamiltonian parameters and their relative orientations are in Table 1 while their relationship to the coordination geometry is in Table 2. The **D**-tensor, derived from the single-crystal study and transformed into the *g*-frame, is in Appendix 1b.

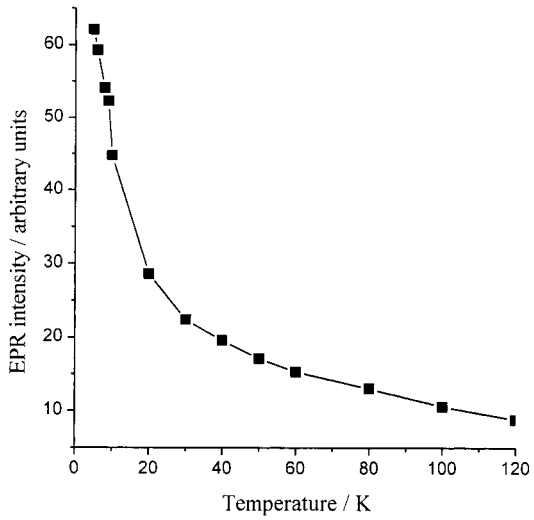

Figure 9. The total relative intensity versus temperature of the K-band EPR powder spectrum of *cis*-$[(NH_3)_2Pt(1\text{-}MeU)_2Cu(H_2O)_2](SO_4)\cdot 4.5H_2O$.

Variable-Temperature Powder Spectra. The total intensity of the powder K-band spectrum increases with decreasing temperature from room temperature to 5 K (Figure 9). Other than in intensity there are no significant changes in the spectra over this temperature range.

Discussion

cis-$[(NH_3)_2Pt(1\text{-}MeU)_2Cu(H_2O)_2](SO_4)\cdot 4.5H_2O$ crystallizes in a head-to-head fashion (Figure 2a) resulting in a weak magnetic exchange interaction between the two copper(II) ions. The lack of a maximum in the EPR intensity versus temperature plot down to 5 K indicates that the isotropic exchange *J* either is ferromagnetic or is weakly antiferromagnetic with a maximum value of ca. 6 cm^{-1} (for a given antiferromagnetic value of *J* in cm^{-1} a maximum is expected at a temperature $T_m \approx |J|/1.112$).[29] A plot of the product of the EPR intensity and the temperature versus temperature decreases continuously with decrease in temperature over the entire temperature range studied, and a plot of $(\text{intensity})^{-1}$ versus temperature can be fit to a Curie−Weiss law with a Weiss temperature of $\theta \approx -5$ K (data not shown). Both of these plots are consistent with a weak antiferromagnetic interaction between the two copper(II) ions. From the experimental EPR spectra $|J|$ must be significantly larger than both the Cu hyperfine (because we observe seven-line multiplets on the low-field features in both the K- and Q-band spectra) and the ZFS interactions (because we observe first-order triplet spectra). Thus, we estimate that $1 < J < 6$ cm^{-1}. This weak interaction between the ground state $d_{x^2-y^2}$ orbitals of the two copper ions is consistent with the structure: the Cu···Cu distance is 3.483 Å, making direct overlap unlikely. The axial−equatorial bridging interaction between the Cu and CuA centers is via O3A. Since O3A cannot overlap with the $d_{x^2-y^2}$ orbital of Cu (and similarly O3 and CuA), there is no superexchange pathway via this ligand. There are no other obvious pathways between the two $d_{x^2-y^2}$ orbitals.

In the absence of a suitable single crystal for EPR studies we attempted to simulate the multifrequency powder spectra

(29) Figgis, B. N.; Martin, R. L. *J. Chem. Soc.* **1956**, 3837.

alone. This was accomplished using a single (i.e., monoclinic) rotation of an axially symmetric **D**-tensor, this rotation being about a direction parallel to the smallest *g*-value (g_{XX}). The rotation angle was 33° ± 2°. This rotation involves an intermixing of the principal value $D_{ZZ} = \mp 0.044$ cm^{-1} with $D_{YY} = \pm 0.022$ cm^{-1}. These simulations account for the positions and relative intensities of the features in the spectra at *all* frequencies, except that marked * in the S-band spectrum. We cannot account for this signal at present.

The simulations of the powder spectra at four different microwave frequencies are good and demonstrate that noncoincidence effects in spin triplet spectra can be detected from multifrequency *powder* EPR measurements.

After we had completed the powder study, we managed to isolate a single crystal of sufficient size and quality to attempt a single-crystal EPR study. This allowed us to test the deductions from the powder data alone and also to determine the orientations of the principal values of the spin-Hamiltonian parameters with respect to the molecular geometry. The single-crystal data reveal that the principal values of the **g**-matrix and **D**-tensor agree well with those determined from the powder data alone (Appendices 1a,b). Moreover, D_{ZZ} is almost in the g_{ZZ}/g_{YY} plane and is at an angle of 33.4° from g_{ZZ}, see Table 1 (g_{XX} and g_{YY} lie approximately along the O4−Cu−O1 and O2−Cu−O3 directions, respectively, see Table 2): this is in remarkable agreement with the angle of noncoincidence determined from powder data alone (33°). However, the relative orientations of the principal values of the **g**-matrix and **D**-tensor are not quite as simple as suggested by the analysis of the powder data: D_{XX} is twisted away from g_{XX} by 32.6° (they are coincident in the simpler model). A comparison of the **D**-tensor derived from the single-crystal data (Appendix 1b) with that from the powder simulations (Appendix 1a) shows that they only differ in the former having small nonzero values of the D_{xy}, D_{yx}, D_{xz}, and D_{zx} elements [when expressed in the *g*-frame (*x*, *y*, *z*)]. The reason for the similarity of the **D**-tensors, and therefore the success of the powder simulations based on a simpler monoclinic model, is that the principal values from the single-crystal study are close to axial. Essentially D_{ZZ} is almost in the g_{ZZ}/g_{YY} plane at 33.4° from g_{ZZ} and 56.6° from g_{YY}. D_{YY} and D_{XX}, which are nearly equal in value, do not lie in the g_{ZZ}/g_{YY} or g_{XX}/g_{YY} planes although D_{YY} is closer to the g_{ZZ}/g_{YY} plane. Thus, the effect of twisting *D* about D_{ZZ} is to mix two numerically similar matrix elements resulting in little change to the *powder* spectra. A representation of the orientations of the **g**-matrix and **D**-tensor relative to the molecular geometry is shown in Figure 2c.

In general, each element of the experimental **D**-tensor has three parts: a dipolar contribution ($\mathbf{D}^{\mathrm{dip}}$), an anisotropic exchange contribution ($\mathbf{D}^{\mathrm{aniso}}$), and an antisymmetric exchange contribution ($\mathbf{D}^{\mathrm{anti}}$). $\mathbf{D}^{\mathrm{anti}}$ is equal to zero because the two Cu centers are centrosymmetrically related.[10] Using the angles between the principal *g*-values and the Cu···CuA vector determined from the single-crystal EPR study (Table 2) we can calculate the $\mathbf{D}^{\mathrm{dip}}$ matrix in the *g*-frame (Appendix 1c). This matrix contains both isotropic and anisotropic components which contribute to *J* and *D*, respectively.[10] The isotropic part is given by the average of the diagonal matrix elements (i.e., one-third of the trace) = +0.0048 cm^{-1}. Subtracting this from each of the diagonal elements gives the anisotropic part of the $\mathbf{D}^{\mathrm{dip}}$ matrix (Appendix 1d), and this matrix is now traceless.

A comparison of the calculated anisotropic dipolar matrix with the experimentally observed **D**-tensor (Appendices 1b,d) suggests that *D* is largely dipolar in origin. This is supported by the fact that D_{ZZ} is approximately collinear with the Cu···CuA vector (D_{ZZ} makes an angle of 3.7° with Cu···CuA). The anisotropic exchange contribution to **D**, $\mathbf{D}^{\mathrm{aniso}}$, can be derived by subtracting the anisotropic dipolar contribution to the calculated dipolar matrix (Appendix 1d) from the experimental *D* data (Appendix 1b) and is given in Appendix 2 for both possible signs of the experimental D_{ij}. All the D_{ij}^{aniso} elements in alternative a in Appendix 2 are very small (≤0.005 cm^{-1}), which would be consistent with *D* being almost entirely dipolar in origin. Alternative b in Appendix 2 has $|D_{ij}^{\mathrm{aniso}}|$ elements an order of magnitude larger, and furthermore the largest elements are the D_{yz}^{aniso} off-diagonal elements. Bencini and Gatteschi have stated that the principal axes of the anisotropic exchange matrix should be parallel to those of the local *g* axes when the **g**-matrices of the two interacting centers are parallel to each other.[10] In the present case the two Cu ions are centrosymmetrically related, and therefore the $\mathbf{D}^{\mathrm{aniso}}$ matrix should be diagonal in the diagonal *g*-frame (*x*, *y*, *z*). Thus we reject alternative b in Appendix 2 and we favor alternative a. This implies that the experimentally observed ZFS is negative in sign: this would be expected for a predominantly dipolar interaction. [Note that, if we perform a similar analysis on the alternative solution of the relative orientations of *g* and *D* with respect to the molecular geometry (where g_{ZZ} makes an angle of 25.6° to the normal of the CuO_4 plane, see Experimental Section), there are very large (>0.1 cm^{-1}) off-diagonal elements in $\mathbf{D}^{\mathrm{aniso}}$.]

Anisotropic exchange has its origins in the combined effects of spin−orbit coupling and exchange interactions between the ground state of one center and the excited state(s) of the second center.[10,11] A quantitative analysis of the anisotropic exchange is difficult, especially when the contributions are small. An expression relating the elements of the $\mathbf{D}^{\mathrm{aniso}}$ matrix to the ground state−excited state exchange interactions has been derived by Kanamori[30] and by Moriya,[31]

$$2D_{kk}^{\mathrm{aniso}} = \sum_{\alpha}\sum_{i}\sum_{j}\frac{\lambda_{\alpha}^{2}\langle g_{\alpha}|\mathbf{L}_{\alpha,k}|e_{\alpha i}\rangle\langle e_{\alpha j}|\mathbf{L}_{\alpha,l}|g_{\alpha}\rangle}{\Delta e_{\alpha i}\Delta e_{\alpha j}} \cdot J(e_{\alpha i}g_{\beta}e_{\alpha j}g_{\beta}) \quad (4)$$

where $\sum_{\alpha}$ is the sum over both centers; g_{α} and e_{α} refer to ground and excited states, respectively; $\sum_i\sum_j$ are sums over all excited states; *k* and *l* are Cartesian components; Δe_{α} are

(30) Kanamori, J. In *Magnetism*; Rado, T. G., Suhl, H., Eds.; Academic Press: New York, 1963; Vol. 1, p 161.
(31) Moriya, T. In *Magnetism*; Rado, T. G., Suhl, H., Eds.; Academic Press: New York, 1963; Vol. 1, p 85. Moriya, T. *Phys. Rev.* **1960**, *120*, 91.

the energy separations between the ground state and excited states e_α; and $J(e_{\alpha i}g_\beta e_{\alpha j}g_\beta)$ is the exchange interaction between the ground state of one center and the excited state of the second center. If we assume that the ligand field on each individual copper center does not cause any d-orbital mixing and that $d_{x^2-y^2}$ is the ground state orbital, the diagonal elements arising from eq 4 can be written as[32]

$$2D_{kk}^{\text{aniso}} = C_k[\Delta g_{kk}]^2 \cdot J(e_\alpha g_\beta e_\alpha g_\beta) \qquad (5)$$

where $\Delta g_{kk} = g_{kk} - 2.0023$ and $C_k = {}^1/_4$ for $k = x$ or y and ${}^1/_{16}$ for $k = z$.

Equation 5 shows that the sign of $J(e_\alpha g_\beta e_\alpha g_\beta)$ is determined by the sign of D_{kk}^{aniso}. Thus for alternative a in Appendix 2, we calculate $J(yz,x^2-y^2,yz,x^2-y^2) \approx +8$ cm^{-1}, $J(xz,x^2-y^2,xz,x^2-y^2) \approx 0$ cm^{-1}, and $J(xy,x^2-y^2,xy,x^2-y^2) \approx -1$ cm^{-1}. Although these values for the ground state−excited state exchange are of the same order of magnitude as the isotropic, ground state−ground state exchange (J), Gatteschi has observed in other Cu(II) dimers that J(ground state−excited state) can be much larger than J(ground state−ground state).[32] Therefore, the values of J(ground state−excited state) determined here are in fact very small and possibly all zero within the limits of the approximations inherent in this treatment. This is consistent with the large Cu···CuA distance and the lack of any suitable superexchange pathways from Cu to CuA via O3 (which lies in nodal planes for the d_{xy}, d_{xz}, d_{yz}, and $d_{x^2-y^2}$ orbitals on CuA). If the anisotropic exchange interaction was significant, we would expect D_{ZZ} to be skewed significantly away from the Cu···CuA vector (indeed, if it was dominant we would expect it to be parallel to g_{ZZ}). Thus, both the isotropic exchange and the ZFS in *cis*-$[(NH_3)_2Pt(1\text{-}MeU)_2Cu(H_2O)_2]_2^{4+}$ are dipolar in origin.

Summary

We have demonstrated the use of multifrequency *powder* EPR spectroscopy, coupled with spectrum simulation, for the detection and quantitative measurement of noncoincidence between the principal axes of the **g**-matrix and ZFS-tensor in the triplet state of a pair of weakly coupled $S = {}^1/_2$ centers in *cis*-$[(NH_3)_2Pt(1\text{-}MeU)_2Cu(H_2O)_2](SO_4)\cdot 4.5H_2O$. We have successfully tested these results by comparison with a single-crystal EPR study, and have shown that the ZFS is almost entirely dipolar in origin.

Although we have applied the method to a well-characterized system, it has the potential to obtain the same information in other $S = {}^1/_2$ dimers. The detection of noncoincidence between the principal axes of the **g**-matrices and **D**-tensors in the triplet state could, in some circumstances, be used to indicate the relative orientations of the centers when no X-ray crystal structure information is available.

Acknowledgment. We are grateful to the EPSRC for funding and to Dr. Madeline Helliwell (Manchester) for indexing a single-crystal for EPR measurements.

(32) Banci, L.; Bencini, A.; Gatteschi, D. *J. Am. Chem. Soc.* **1983**, *105*, 761. Banci, L.; Bencini, A.; Gatteschi, D. *Inorg. Chem.* **1984**, *23*, 2138.

Appendix 1. D (cm^{-1}) Matrices Expressed in an Axis System Parallel to the Local Copper Atom *g*-Frame

(a) From powder simulations alone:

$$\begin{array}{c} \\ x \\ y \\ z \end{array} \begin{array}{c} \begin{array}{ccc} x & y & z \end{array} \\ \begin{pmatrix} \pm 0.022 & 0 & 0 \\ 0 & \pm 0.003 & \pm 0.030 \\ 0 & \pm 0.030 & \mp 0.025 \end{pmatrix} \end{array}$$

The principal elements of the diagonalized **D**-tensor are $D_{XX} = \pm 0.022$, $D_{YY} = \pm 0.022$, $D_{ZZ} = \mp 0.044$ cm^{-1}. This is equivalent to an Euler angle of 33° about x.

(b) From single-crystal EPR measurements:

$$\begin{array}{c} \\ x \\ y \\ z \end{array} \begin{array}{c} \begin{array}{ccc} x & y & z \end{array} \\ \begin{pmatrix} \pm 0.0222 & \pm 0.0011 & \pm 0.0002 \\ \pm 0.0011 & \pm 0.0026 & \mp 0.0298 \\ \pm 0.0002 & \mp 0.0298 & \mp 0.0249 \end{pmatrix} \end{array}$$

The principal **D** elements are $D_{XX} = \pm 0.0228$, $D_{YY} = \pm 0.0211$, $D_{ZZ} = \mp 0.0439$ cm^{-1}.

(c) Point-dipole contribution $\mathbf{D}^{\text{dip}}$ calculated from the single-crystal diffraction data and the direction cosine matrix between the principal *g*-values and the Cu···CuA vector:

$$\begin{array}{c} \\ x \\ y \\ z \end{array} \begin{array}{c} \begin{array}{ccc} x & y & z \end{array} \\ \begin{pmatrix} +0.0219 & +0.0023 & +0.0040 \\ +0.0023 & +0.0075 & -0.0259 \\ +0.0040 & -0.0259 & -0.0150 \end{pmatrix} \end{array}$$

This matrix is not traceless because of *g*-anisotropy on the individual copper centers.

(d) Anisotropic dipolar contribution to the calculated $\mathbf{D}^{\text{dip}}$ tensor:

$$\begin{array}{c} \\ x \\ y \\ z \end{array} \begin{array}{c} \begin{array}{ccc} x & y & z \end{array} \\ \begin{pmatrix} +0.0171 & +0.0023 & +0.0040 \\ +0.0023 & +0.0027 & -0.0259 \\ +0.0040 & -0.0259 & -0.0198 \end{pmatrix} \end{array}$$

Appendix 2. The Two Alternative D_{ij}^{aniso} Matrices Calculated from the Single-Crystal EPR Data and the Calculated Anisotropic Point-Dipole Contribution

The $\mathbf{D}^{\text{aniso}}$ matrices are expressed in an axis system parallel to the local copper atom *g*-frame, and the elements are in cm^{-1}.

(a)

$$\begin{array}{c} \\ x \\ y \\ z \end{array} \begin{array}{c} \begin{array}{ccc} x & y & z \end{array} \\ \begin{pmatrix} +0.0051 & -0.0013 & -0.0038 \\ -0.0013 & -0.0001 & -0.0039 \\ -0.0038 & -0.0039 & -0.0052 \end{pmatrix} \end{array}$$

(b)

$$\begin{array}{c} \\ x \\ y \\ z \end{array} \begin{array}{c} \begin{array}{ccc} x & y & z \end{array} \\ \begin{pmatrix} -0.0393 & -0.0034 & -0.0042 \\ -0.0034 & -0.0053 & +0.0557 \\ -0.0042 & +0.0557 & +0.0447 \end{pmatrix} \end{array}$$

IC011283E